RSC Advances

PAPER

View Article Online
View Journal | View Issue

Cite this: *RSC Adv.*, 2023, **13**, 2501

Effect of regio-specific arylamine substitution on novel π-extended zinc salophen complexes: density functional and time-dependent density functional study on DSSC applications†

Jian-Ming Liao, Yu-Kai Chin, Yu-Ting Wu and Hsien-Hsin Chou *

A series of π-extended salophen-type Schiff-base zinc(II) complexes, *e.g.*, zinc-salophen complexes (ZSC), were investigated toward potential applications for dye-sensitized solar cells. The ZSC dyes adopt linear-, X-, or π-shaped geometries either with the functionalization of 1 donor/1 acceptor or 2 donors/2 acceptors to achieve a push–pull type molecular structure. The frontier molecular orbitals, light-harvesting properties as well as charge transfer characters against regio-specific substitution of donor/acceptor groups were studied by using density functional theory (DFT) and time-dependent density functional theory (TDDFT). The results reveal that all ZSC dyes of D-ZnS-π-A geometry (where D, S, and A denote to donor, salophen ligand, and acceptor, respectively) exhibit relatively lower HOMO energy compared to the structurally resembled porphyrin dye **YD2-*o*-C8**. Natural transition orbital (NTO) and electron–hole separation (EHS) approaches clearly differentiate the linear type **YD**-series dyes from **CL**-, **AJ1**-, and **AJ2**-series dyes because of poor charge transfer (CT) properties. In contrast, the π-shaped **AJ2**-series and X-shaped **AJ1**-series dyes outperform the others in a manner of stronger CT characteristics, broadened UV-vis absorption as well as tunable bandgap simply *via* substitution of *p*-ethynylbenzoic acids (EBAs) and arylamine donors at salophen 7,8- and 2,3,12,13-positions, respectively. Both EHS and calculated exciton binding energies suggest the strength of CT character for ZSC dyes with an amino donor in the trend TPA > AN > DPA. This work has provided clear illustration toward molecular design of efficient dyes featuring a zinc-salophen backbone.

Received 28th November 2022
Accepted 4th January 2023

DOI: 10.1039/d2ra07571g

rsc.li/rsc-advances

Introduction

The two most imperative changes the world has faced in recent years are the global pandemic of coronavirus disease (COVID-19) and the urgent need for alternative energy sources. The third-generation photovoltaic technologies,[1] including perovskite solar cells (PSCs),[2,3] dye-sensitized solar cells (DSSCs),[4,5] organic photovoltaics (OPVs),[6,7] and quantum dot solar cells (QDSCs),[8,9] are some of the fast growing energy technologies in the world. The high flexibility in size, shape, and color, as well as high-efficiency indoor applications account for the fascinating features of these solar cell technologies. Unfortunately, so far none of these solar cell techniques dominate mass production for end-use applications. The DSSC technologies are considered to be of greater potential because of lower cost, reasonable stability, high performance under dim-light environments,[10] and tolerability toward integration with other technologies such as energy storage.[11] Due to the multiple electron transfer processes[4,12,13] at dramatically different timescales involved in the operation principle of DSSC, a sophisticated balance between each process will undoubtedly determine high performance of the device. As shown in Fig. 1, the dye photosensitizer plays imperative role since electric power conversion can be tuned *via* molecular geometry which eventually lead to optimized properties such as frontier molecular orbitals, redox potentials, intramolecular charge-transfer (ICT) excitations, reorganization energies, and so on,[12,13] as annotated in arrows A-C in the figure. Modern state-of-the-art dyes for DSSCs, such as **GY50** [14](PCE = 12.75%; V_{OC} = 0.89 V; J_{SC} = 18.53 mA cm^{-2}; FF = 0.77), **SM315** [15](PCE = 13.0%; V_{OC} = 0.91 V; J_{SC} = 18.1 mA cm^{-2}; FF = 0.78), **SGT-021** [16](PCE = 12.0%; V_{OC} = 0.91 V; J_{SC} = 17.5 mA cm^{-2}; FF = 0.75), **XW61** [17](PCE = 12.4%; V_{OC} = 0.78 V; J_{SC} = 21.4 mA cm^{-2}; FF = 0.75), and **bJS2** (PCE = 10.69%; V_{OC} = 0.85 V; J_{SC} = 16.6 mA cm^{-2}; FF = 0.76)[18] adopt push–pull type molecular geometry using zinc-porphyrin as molecular backbone together with arylamino donor and LBG-benzoic acid groups, where LBG denotes to low-bandgap groups such as benzothiadiazole and diketopyrrolopyrrole.[14,18,19] Compared with push–pull type

Department of Applied Chemistry, Providence University, Taichung 43301, Taiwan. E-mail: hhchou@pu.edu.tw

† Electronic supplementary information (ESI) available: Experimental details, NMR spectra, calculated frontier molecular orbitals, angles, and predicted spectra (PDF). See DOI: https://doi.org/10.1039/d2ra07571g

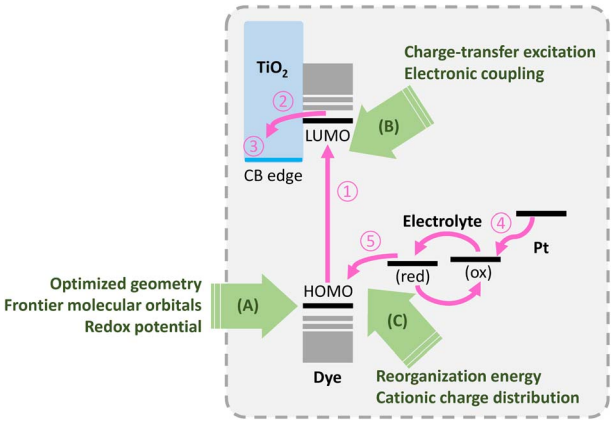

Fig. 1 Working principle of DSSC. The electron transfer processes are noted as: (1) light harvesting, (2) electron injection, (3) charge transport, (4) electrolyte regeneration, (5) dye regeneration.

porphyrin-based dyes,[20,21] organic dyes are commonly constructed with donor–π bridge–acceptor (D–π–A) and donor–acceptor-π bridge-acceptor (D-A-π-A) configuration in order to have promising light-harvesting properties as well as easily modified molecular structure for reduced charge recombination.[22] Here the D (electron-donating group) and neighboring A (electron-deficient group) often feature arylamines and low-bandgap chromophores, respectively. The molecular design of donor–acceptor (D–A) backbone enhances intramolecular charge transfer (ICT) character which is beneficial to broadened absorption spectrum and eventually the short-circuit current density (J_{SC}). The same design has also proven successful in the field of perovskite solar cell technologies in terms of increased hole extraction and reduced exciton recombination rate.[23,24] Despite the extensive absorption at UV-vis region, the high efficiency achieved by porphyrin dyes can be rationalized by the employment of cobalt(II/III)-based redox electrolyte for increased V_{OC}, owing to relatively positive redox potential.[25] Finally, another important thing to achieve high performance is inhibition of excessive recombination to electrolyte (either iodide-based or cobalt-based) in oxidized form.[26,27] This can be achieved *via* "surface passivation" typically using (1) co-adsorbent or co-sensitizer,[28] (2) additives in the electrolytes such as *t*-BP[29] and GuSCN,[30] (3) atomic layer deposition of low work function oxide such as Al_2O_3 and[31] La_2O_3,[32] (4) *via* functionalizing aliphatic chains on the dye molecules to form "insulation layer",[33] and (5) duplicate anchor sites on the dye molecules to exclude the electrolytes from the proximity of TiO_2 surface nearby the anchor.[34–39] Although many high-efficiency dyes with sophisticated molecular design have been reported, these dyes suffer from major drawback of excessive synthetic procedures. More than 20 steps starting from the most simplest commercially available chemicals are practically required. The need for seeking relatively simple yet cost-efficient molecular design of dyes thus arose.

Interestingly, although the porphyrin-based dyes featuring *N*,*N*,*N*,*N*-tetradentate molecular framework have been extensively investigated, studies relating structurally resembled dyes based on *O*,*N*,*N*,*O*-tetradentate salophen-type Schiff-based metal complex are found rare.[40–43] The metal-salophen complexes have strong UV-Vis absorption with broad spectral coverage which meet the principal criteria of a light harvesting photosensitizer.[28] In addition, the molecular properties can be easily manipulated *via* tuning the frontier molecular orbitals, charge-transfer characteristics, and probably other intermolecular interactions and potential catalytic properties.[44–46] Jing and coworkers developed a new class of D–π–A type sensitizers (**SLa-SLf**) based on zinc(II)-salophen complexes (ZSC), where D and A denote to arylamino and carboxylic substituents at salophen 5,5′-positions. These dyes exhibit extensive π–π* transition and weak charge transfer absorption at 300–350 nm ($\varepsilon = ca.$ 1×10^5 M^{-1} cm^{-1}) and 400–600 nm ($\varepsilon = ca.$ 2×10^4 M^{-1} cm^{-1}), respectively. However, DSSCs fabricated with these dyes reach the best photovoltaic performance of 0.81% under illumination of AM 1.5G standard condition (100 mW cm^{-2}), with poor open-circuit voltage (V_{OC}) and short-circuit current density (J_{SC}) of 0.62 V and 1.85 mA cm^{-2}, respectively. Similar results were obtained for Pt- and Zn-derivatives where donor groups are functionalized at salophen 4,4′-positions.[42] The power conversion efficiency (PCE) account for these Pt- and Zn-based dyes are 1.53% and 0.99%, respectively. The poor performance of these dyes is probably attributed to (1) the relative higher HOMO level, (2) close proximity of arylamines to TiO_2 surface leading to increased charge recombination from TiO_2 to oxidized dyes and redox electrolytes, and (3) perhaps together with the series dye aggregation. To effectively control the molecular properties of the ZSC dye, a sophisticated design of molecular structure is definitely required. Consequently, the need for scrutinizing the structure–property relationship for MSC molecules thus arose. Herein, we report a density functional and time-dependent density functional investigation based on newly proposed structures involving zinc–salophen complex (ZSC) as molecular building blocks. Unlike traditional linear push–pull type molecular design, these complexes are of D–π–A or D_2–π–A_2 geometry where ZSC services as a bridging π unit that can simultaneously trigger molecular properties simply *via* regio-specific substitution. The results have clearly lead to useful guidelines regarding molecular design of efficient photosensitizers containing the zinc-salophen backbone.

Results and discussion

Fig. 2 shows the molecular structure for a series of D–π–A and D_2–π–A_2 type dyes under investigation, together with the reference dye **YD2-*o*-C8**. All dyes are highly π-extended molecules where the zinc-salophen (ZnS) framework is functionalized with arylamine(s) and *p*-ethynylbenzoic acid(s) at specific positions as donor and acceptor groups, respectively. The influence of *p*-ethynylbenzoic acid (EBA) have proven to be beneficial to better light-harvesting and J_{SC} increment.[47–49] These dyes are categorized into **YD**-, **CL**-, **AJ1**-, and **AJ2**-series, each being tethered with donor groups such as dialkylaniline (AN), diphenylamine (DPA), and triphenylamine (TPA) in order to probe the substituent effect. Dyes **YD-AN**, **YD-DPA**, and **YD-TPA** each possess a linear push–pull type geometry where donor

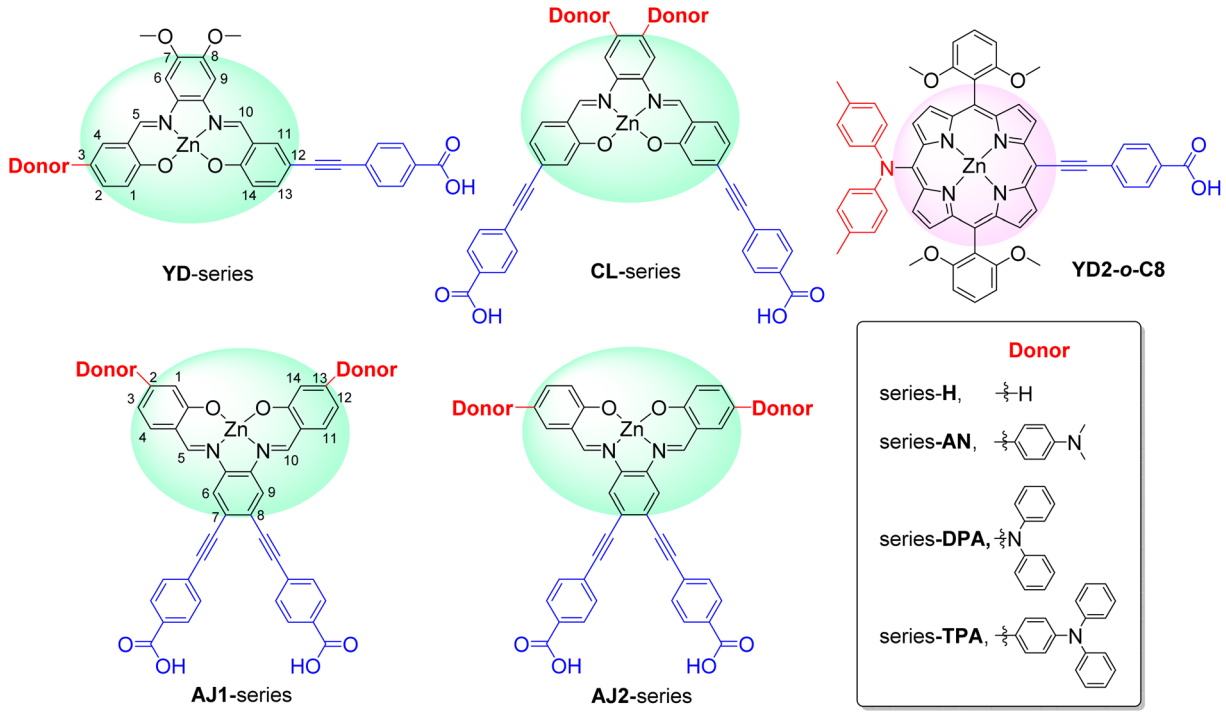

Fig. 2 Molecular structures of ZSC dyes based on zinc-salophen complexes. Note: **AJ1-H** and **AJ2-H** refer to the same dye.

and acceptor groups are in the 3,12-position, a resultant molecule that is structurally resemble the state-of-the-art porphyrin dyes such as **YD2-*o*-C8**.[50] Note that two additional methoxy groups were functionalized at 7,8-position. The tetra-substituted dyes **CL-AN**, **CL-DPA**, and **CL-TPA** have donors and acceptors functionalized at 7,8- and 2,13-position of ZnS core, respectively, to furnish an "X"-shape molecular framework. Another series of X-type dye are **AJ1**-derivatives containing position-swapped donors and acceptors. The **AJ2**-series dyes, on the other hand, are tetra-substituted ZSC complexes with "π"-shape geometry where donors and acceptors tethered at 3,12- and 7,8-positions, respectively. The molecular design with dual anchor[17,35–37,39] have proven to improve stability on TiO_2 surface as well as performance parameters such as V_{OC}.[38,51] Fig. 3 displays the atom-by-atom superimposition of ZSC dyes optimized at B3LYP/6-311G(d,p) level of theory. The result reveals a twisted tetrahedral geometry surrounding the *N*,*N*,*O*,*O*-tetra-coordinated zinc centers for all ZSC dyes. Coordination of additional pyridine on zinc center leads to molecular geometry of distorted square pyramid (shown as sideview in Fig. 3). The later results meet the reported observations from crystal structural determination, where ZSC adopts distorted square pyramidal geometry with one coordinating solvent molecule bonded to zinc ion, such as DMSO,[52] water,[53] and pyridine.[54] We noted that inclusion of diffusion functions, *e.g.*, 6-311+G(d,p), for optimizing the solvent-free molecules lead to distorted square planar geometry, which differs from distorted square pyramid reported in the literature using 6-311++G(d,p) (with unclear calculation detail).[53] Consequently, the basis sets without diffusion function and pseudopotentials were used throughout this study. Furthermore, each dye molecule possesses highly planar conjugation at ethynylbenzoic acid groups (EBAs), indicating that remarkable π–π* transitions with large extinction coefficient can be envisioned for ZSC dyes (Fig. S1 and S2†). This is believed to contribute to better UV-vis spectral response through enhanced π-conjugation.

Fig. S3† illustrates frontier molecular orbitals for all dyes in this study. The energy levels regarding lowest unoccupied molecular orbitals (LUMOs) are of the range between −2.37 and −2.83 eV, allowing for sufficient driving forces toward electron injection into TiO_2 conduction band. The highest occupied molecular orbitals (HOMOs) are of the energies between −4.94 and −5.76 eV, and are largely stabilized compared to theoretically optimized **YD2-*o*-C8** (−4.83 eV). This fact is beneficial to larger theoretical open-circuit voltage (V_{OC}) such that redox electrolytes with satisfactorily lower redox potential can be used, *e.g.*, the cobalt-[18,50,55] and copper-based complexes.[56–60] In general, the HOMOs predominately populated at ZnS and arylamine moieties, whereas LUMOs mainly at ZnS and EBA moieties (Fig. S3†). Consequently, the lowest-energy vertical excitations will exhibit significant charge transfer character leading to effective electron injection from photoexcited dye to TiO_2 conduction band (see also Fig. 1).[61,62] We noted that the TPA-substituted dyes encompass minimized HOMO contribution from ZSC moiety compared to DPA- and AN-derivatives, which is possibly a consequence of prolonged π-extension across the twisted biphenyl linkage. (Fig. S1†). Nonetheless, the TPA-containing dyes are prone to have higher HOMO levels in accompanied with significant charge transfer behavior upon vertical excitation, as will be discussed later. Fig. 4 and Table S1† compares the HOMO energies for all pyridine-free ZSC dyes, together with a primitive ZSC molecule, **ZSHH** (−5.36 eV), and

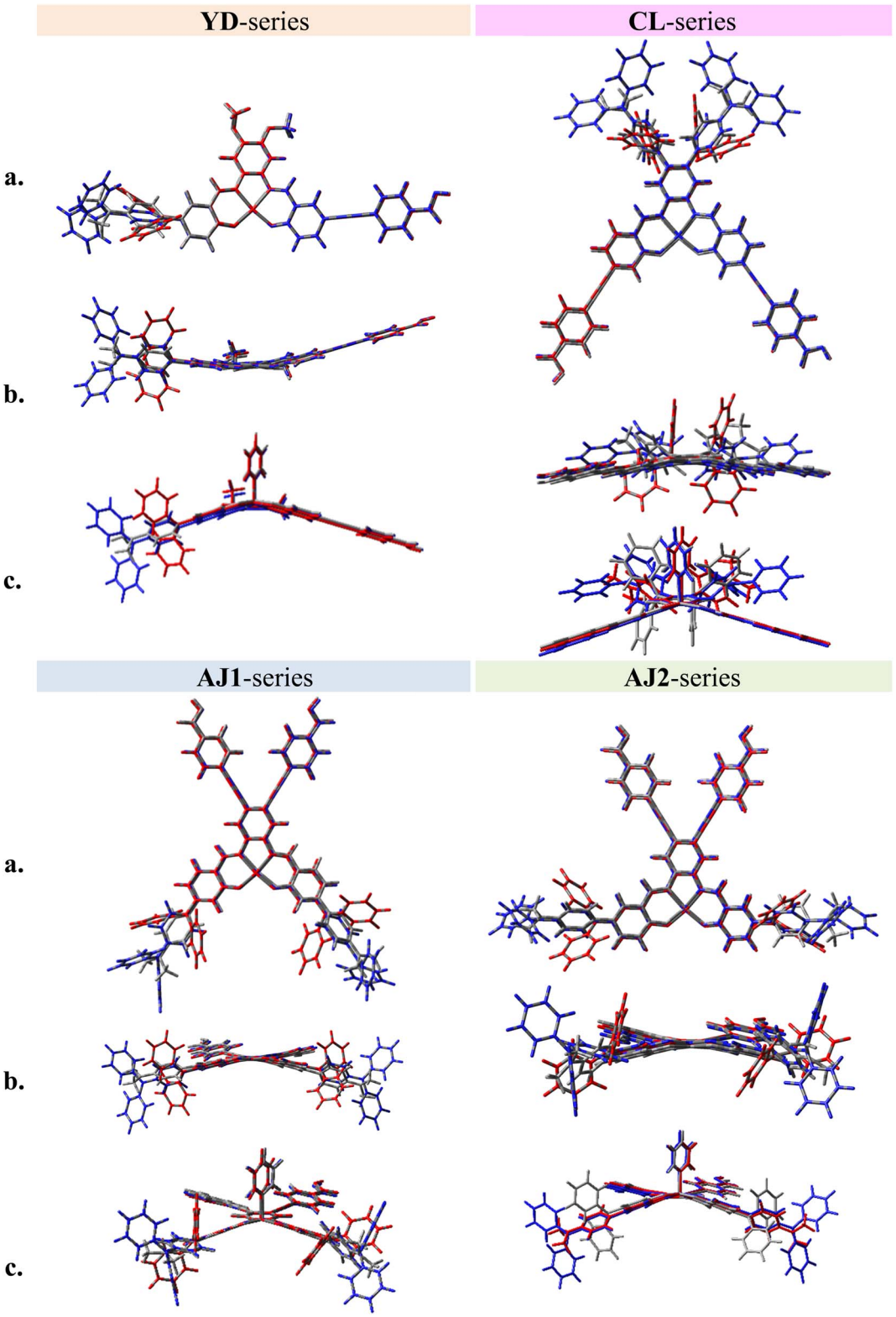

Fig. 3 Atom-by-atom superimposition of the optimized molecular geometries for ZSC dyes from (a) top view, (b) side view, and (c) side view (with pyridine coordinated on Zn center). Those in gray represent series-AN dyes, while that in red and blue represent series-DPA and series-TPA dyes, respectively.

the reference porphyrin dye **YD2-*o*-C8** (−4.83 eV). In the case where donor groups are absent, dyes **YD-H** (−5.44 eV) and **AJ1-H** (also named as **AJ2-H**; −5.69 eV) have slightly elevated HOMO energy compared to **CL-H** (−5.76 eV), indicating more pronounced acceptor influence when substituted at 2,13-position. In fact, the HOMO energies for **CL**-series dyes are also

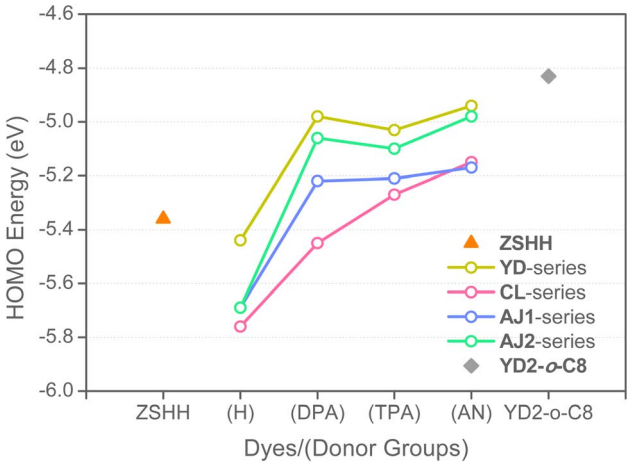

Fig. 4 Elevation of HOMO energy for YD-, CL-, AJ1- and AJ2-series dyes. Results were conducted at B3LYP/6-311G(d,p) level of thery.

largely affected by substituted donor groups at 7,8-position: **CL-H** (−5.76 eV) < **CL-DPA** (−5.45 eV) < **CL-TPA** (−5.27 eV) < **CL-AN** (−5.15 eV). On the other hand, the **YD-** (−4.94 to −5.03 eV), **AJ1-** (−5.17 to −5.22 eV) and **AJ2**-series (−4.98 to −5.06 eV) dyes generally have higher-lying HOMOs which are relatively unaffected by substituted donor groups. Furthermore, the donor influence is becoming more pronounced when substituted at 2,13-position rather than 3,12-position, *e.g.*, **AJ1-DPA** (−5.22 eV) < **AJ2-DPA** (−5.06 eV) ≈ **YD-DPA** (−4.98 eV), **AJ1-TPA** (−5.21 eV) < **AJ2-TPA** (−5.10 eV) ≈ **YD-TPA** (−5.03 eV), and **AJ1-AN** (−5.17 eV) < **AJ2-AN** (−4.98 eV) ≈ **YD-AN** (−4.94 eV). The position-sensitive HOMO energies for ZSC dyes can be envisaged when comparing the difference in HOMO population at salophen ligand (Table S1†). Interestingly, the relationship between HOMO energies and lowest-energy ($S_0 \rightarrow S_1$) vertical excitation energies (E_{cal}) also show regio-specificity (*vide infra*).

TDDFT calculations for dyes in this study were conducted to understand the structure–property relationships concerning UV-vis absorption behavior together with underlying charge transfer characteristics. To ensure reasonable prediction of photoexcitation properties without excessive methodological studies, we carried out synthesis of a primitive zinc–salophen complex, **ZSHH6**, with dihexyloxy substitution at 7,8-position (detailed in ESI†) followed by optimizing the calculation methods *via* fitting the results to experimental observations. As shown in Scheme S1,† the catechol first underwent alkylation with 1-bromohexane in acetone. The resulting *o*-dihexyloxybenzene (A) was then treated with nitric acid to form dinitro-derivatives (B). Further reduction of nitro groups with hydrazine catalyzed by palladium on carbon followed by condensation with salicylaldehyde in the presence of zinc acetate gave the desired zinc–salophen complex (**ZSHH6**) as orange microcrystals. The compound has been characterized *via* ^{1}H NMR and ^{13}C NMR (detailed in ESI†). Like the methoxy derivatives,[63] the UV-vis absorption spectrum of **ZSHH6** in THF shows broad absorption peaks at 356, 411, and 445 nm with strong extinction coefficient of 2.75 × 10^4, 3.72 × 10^4, and 2.21 × 10^4 M^{-1} cm^{-1}, respectively (Fig. S4a†). On the other hand, TDDFT calculations were conducted for model compound **ZSHH** where excess alkyl groups being truncated. The basis sets including 6-31G(d) and 6-311G(d,p) were employed for calculation, while hybrid (B3LYP) and long-range-corrected functionals were tested. Fig. 5 displays the experimental UV-vis absorption in THF fitted by convoluted excitation peaks of TDDFT results. The conventional hybrid B3LYP functional with a constant fraction of HF exchange shows adequate prediction with three absorption peaks at 352, 392, and 461 nm. However, the range-separated functionals including LC-PBE0, wB97XD, and LC-BLYP show great deviation from experimental result when using default value of range–separation parameter ω (shown as dashed lines in Fig. 4). The reason might be the incorrect asymptotic behavior of exchange-correlation potential originated from inappropriate separation criteria for short-range (SR) and long-range (LR) parts of Coulomb potential operator which eventually leads to overestimation of excitation energies.[64] On the other hand, tuning the ω value by using Koopmann's theorem[65,66] for error function used in LRC scheme gives moderate (in the case of LC-PBE0 and wB97XD) to good (in the case of LC-BLYP) approximation results. The later shows simulated absorption at 332, 354, and 441 nm. Note that the employment of solvation model mainly results in stronger oscillator strength for each excitation without significant change in excitation energy (Fig. S4b†). Additionally, the relative low-cost time-dependent ZINDO calculation[67,68] on compound **ZSHH** were also tested with and without solvation model. Overestimation of excitation energy and absorption intensity was observed for charge-transfer and local-excitations peaks, respectively, compared to experimental results (Fig. 5 and S4b†). According to the aforementioned results, a hybrid (B3LYP) and tuned range-separated (LC-BLYP) functional were used for further gas phase calculations on ZSC molecules, as shown in Fig. 6a and b, respectively. The predicted results show

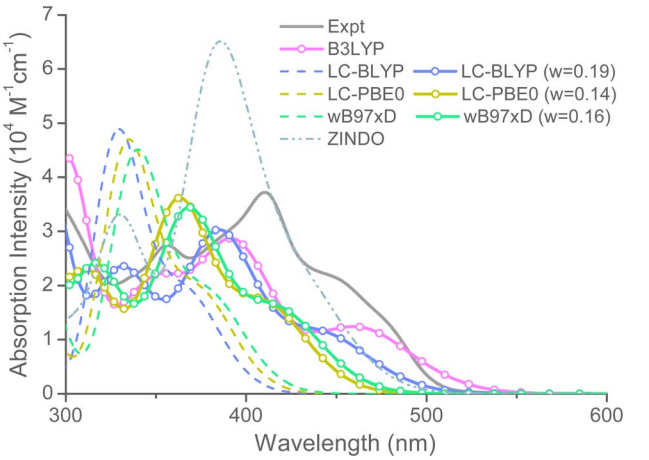

Fig. 5 Comparison between experimental (gray line) and simulated UV-vis absorption spectra for **ZSHH**. The 6-31G* basis set were employed. All calculations were conducted in gas phase. By default (dashed line), the LRC functional have ω values of 0.47, 0.30, and 0.30 for LC-BLYP, LC-PBE0, and wB97XD, respectively.

that all dyes possess broad absorption spanning from 300 nm to >550 nm with two prominent absorption maxima, regardless of the choice of functional. Like that reported in the literature, the porphyrin analogues with multiple D/A substituents (**CL**-, **AJ1**-, and **AJ2**-series) exhibit better light harvesting than single D/A derivatives, *e.g.* **YD**-series.[51,69,70] The lower-lying absorption maximum (λ_{max}) at 400–700 nm are π–π* excitation with significant charge transfer character ($S_0 \rightarrow S_n$, $n = 1$–4 for **YD**-, **CL**-, and **AJ2**-dyes; $n = 1$–8 for **AJ1**-dyes), while the higher-lying absorption peaks located at 300–400 nm appear to be localized π–π* excitation ($S_0 \rightarrow S_n$, $n = 5$–20). Additionally, the predicted absorption coefficient for λ_{max} reveals a trend of **AJ1** ($\varepsilon > 10^5$ M^{-1} cm^{-1}) > **CL** ($\varepsilon > 5 \times 10^4$ M^{-1} cm^{-1}) > **YD** ≈ **AJ2** ($\varepsilon < 5 \times 10^4$ M^{-1} cm^{-1}). Finally, more red-shifted λ_{max} were predicted for **AJ2**-series dyes at 500–700 nm using B3LYP functional. The is believed to be originated from π-shape geometry of the dye, as will be elucidated later. Overall, these observations have concluded that the π-type **AJ2**-series dyes exhibit broader absorption while the X-type **AJ1**-series dyes have more extensive charge transfer excitation. Note that in the presence of coordinating pyridine, a blue-shifted absorption was observed for **AJ2**-series dyes, possibly due to changes in charge transfer behavior (Fig. S5†).

Upon illumination of sunlight, *e.g.*, at standard AM 1.5G condition, higher J_{SC} values of the device require optimization of factor including light-harvesting efficiency (LHE), electron-

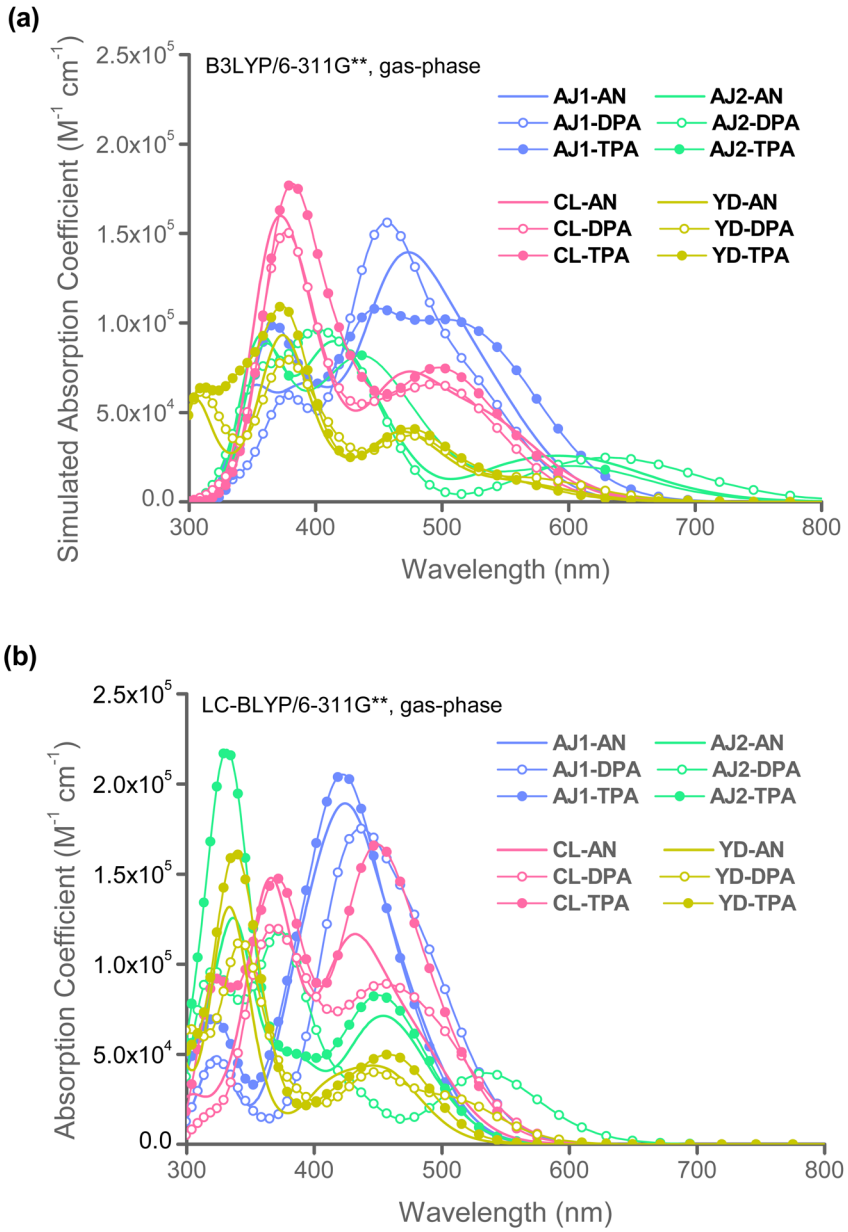

Fig. 6 Simulated UV-vis absorption spectra for **YD**-, **CL**-, **AJ1**-, and **AJ2**-series dyes using 6-311G(d,p) basis set and (a) B3LYP as functional; (b) tuned LC-BLYP as functional.

injection efficiency (η_{inj}), charge-collection efficiency (η_{col}), dye-regeneration efficiency (η_{reg}), and photon flux ($\Phi(\lambda)$), as shown in eqn (1),

$$J_{SC} = \int \mathrm{LHE} \cdot \eta_{inj} \cdot \eta_{col} \cdot \eta_{reg} \cdot \Phi(\lambda) \mathrm{d}\lambda \quad (1)$$

Table 1 lists one of the key parameters, LHE,[71–73] calculated according to eqn (2),

$$\mathrm{LHE} = 1 - 10^{-f} \quad (2)$$

where f is the oscillator strength for the corresponding major excitation contributed to the absorption maximum. The result shows that LHE values for all ZSC dyes are in the range between 76% and 94% at the major absorption (localized π–π^*) region, while in the case of CT region, LHE are roughly of the trend **AJ1** dyes (73–94%) > **CL** dyes (57–76%) ≈ **YD** dyes (61–65%) >> **AJ2** dyes (32–36%). In the case of **AJ2** dyes the relatively lower LHE is possibly attributed to poor special overlap of orbitals involved in the electronic transition, as will be illustrated in the following section. Table 2 further summarizes the lowest-energy TDDFT results for ZSC dyes in this study together with particle-hole excitation scheme calculated using natural transition orbitals (NTOs). The results show large variation for calculated lowest-energy excitation energy (E_{cal}) ranging from 1.882 to 2.354 eV, corresponding to predicted λ_{max} of *ca.* 527 to 659 nm. These dyes exhibit different relationships between the calculated E_{cal} and the corresponding HOMO energies, depending on the choices and positions of donor/acceptor groups. As shown in Fig. 7, in the case of **CL**- and **YD**-series dyes where EBAs are functionalized at phenoxide 3,12,2,13-positions, the donor substituents significantly affect HOMO energies (for **CL**-series) while only perturb E_{cal} (for both series). On the contrary, for both **AJ1**- and **AJ2**-series dyes where EBAs are substituted at phenylenediimine 7,8-position, the substituted donor groups greatly change E_{cal} but slightly alter the HOMO energies. Considering that all the ZSC dyes already have sufficiently lower-lying HOMO levels (*vide supra*), the X-type **AJ1**-series and π-type **AJ2**-series dyes would therefore be better dye candidates owing to easy manipulation of light-harvesting properties. We noted that Janssen and coworkers[74] reported a correlation between bandgap (either optical or electrochemical) and HOMO energy for the diketopyrrolopyrrole-dithienopyrrole copolymer system. The calculated smaller effective exciton binding energy (E_{eb})[75,76] was proven to correlate with stronger push–pull character exerted by the molecule. However, in our case there shows no clear relationship between E_{eb} and HOMO energy nor vertical excitation energy (*vide infra*). Moreover, the most striking feature found for **YD**-series dyes was their lowest-energy NTOs. Charge transfer (CT) excitations occur between arylamino donor and ZnS skeleton, while in the cases of dyes other than **YD**-series, CT occur between arylamines and EBAs with partial overlap at ZnS moiety. That is, the lowest-energy excitation of **YD**-series dyes are unable to facilitate electron injection into TiO_2 semiconductor. In fact, only the $S_0 \rightarrow S_n$ excitations ($n > 4$) that involves LUMO+2 would lead to sufficient electron injection (Tables S1 and S2†). As a comparison, **YD2-*o*-C8**, the highly efficient porphyrin dye of D–ZnL–π–A geometry (where L = ligand complexed on Zn^{2+}) exhibits effective donor-to-anchor/acceptor CT excitation at states as low as $S_0 \rightarrow S_1$.[47,77] We further calculated the exciton binding energies (negative value of Coulomb attractive energies), E_{eb},[75,76] between the holes and electrons for ZSC dyes. The smaller E_{eb} indicates the stronger CT character represented by the dye molecule. Here the calculated trend for substituted arylamino donors is TPA-derivatives (1.66–2.10 eV) < AN-derivatives (2.09–2.38 eV) < DPA-derivatives (2.34–2.83 eV), which also echo the predicted absorption behavior mentioned earlier (Fig. S6†). The intramolecular charge transfer behavior determined by electron–hole separation (EHS)[78] further confirms this observation (Table 1, columns 1–3 from the right). Again, the depletion and increment of electron density occurs as a localized CT process for the **YD**-series dyes, while that for the other dyes have CT processes featuring sufficient electron injection. The DPA-containing dyes exhibit relative shorter charger transfer distances (L) compared

Table 1 Parameters relating TDDFT calculations of the dyes

Dye series donor		Use major absorption peak				Use maximum absorption peak			
		State	E_{cal} (eV)	f^a	LHE^b	State	E_{cal} (eV)	f^a	LHE^b
YD-series	AN	S7	3.30	0.88	0.870	S3	2.66	0.45	0.644
	DPA	S7	3.30	0.71	0.804	S3	2.60	0.45	0.649
	TPA	S8	3.31	1.25	0.944	S3	2.63	0.41	0.612
CL-series	AN	S15	3.41	0.75	0.823	S3	2.63	0.62	0.758
	DPA	S11	3.29	0.62	0.761	S2	2.47	0.37	0.573
	TPA	S12	3.23	0.69	0.798	S3	2.49	0.50	0.685
AJ1-series	AN	S5	2.68	0.92	0.880	S5	2.68	0.92	0.880
	DPA	S3	2.67	1.22	0.939	S3	2.67	1.22	0.939
	TPA	S7	2.80	1.09	0.919	S3	2.45	0.56	0.727
AJ2-series	AN	S11	3.00	0.78	0.833	S4	2.24	0.19	0.358
	DPA	S11	3.12	0.91	0.877	S1	1.88	0.17	0.331
	TPA	S9	2.84	0.81	0.846	S1	2.00	0.17	0.325

[a] Oscillator strength. [b] Light-harvesting efficiency calculated using the formula $\mathrm{LHE} = 1 - 10^{-f}$, where f is the largest absorption intensity (oscillator strength) of the sensitizer at major or maximum absorption peaks.

Table 2 Natural transition orbitals (NTOs) and electron–hole separations (EHS) of the first excited states in ZSC dyes[a]

Dye	E_{cal}[b] (eV)	NTO[c] Hole	NTO[c] Electron	NTO[c] Population	E_{eb}[d] (eV)	EHS[e]	EHS[e] L (Å)	EHS[e] t (Å)
YD-AN	2.215	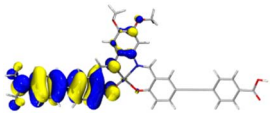	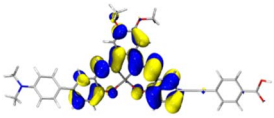	99.4%	2.381	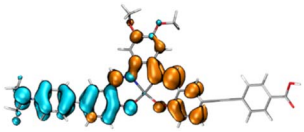	7.489	4.005
YD-DPA	2.157	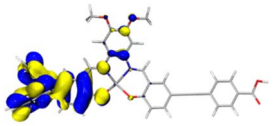	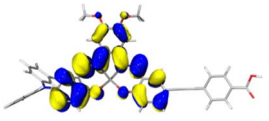	98.8%	2.830	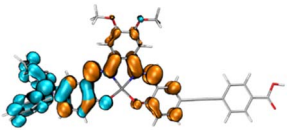	5.401	2.185
YD-TPA	2.265	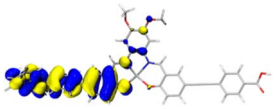	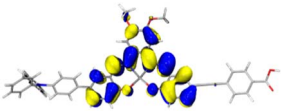	99.3%	2.098	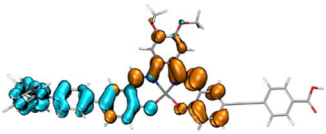	8.668	4.780
CL-AN	2.257	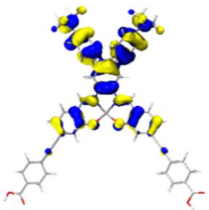	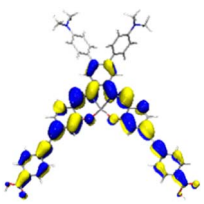	99.4%	2.161	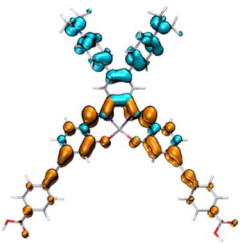	6.445	2.450
CL-DPA	2.316	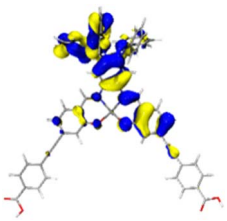	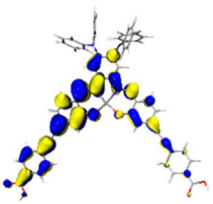	99.1%	2.490	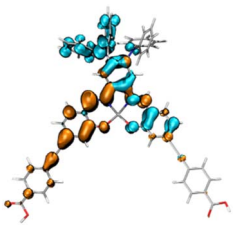	4.887	1.234
CL-TPA	2.265	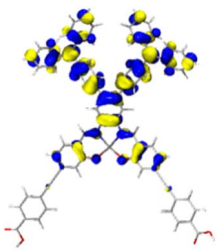	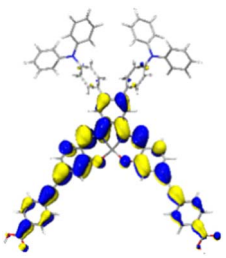	99.4%	1.890	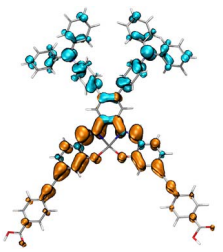	7.868	3.783
AJ1-AN	2.303	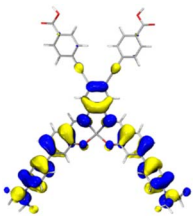	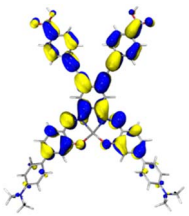	99.3%	2.085	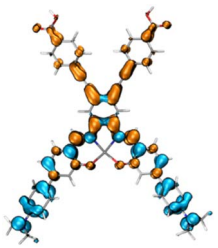	6.201	1.679

Table 2 (*Contd.*)

Dye	E_{cal}[b] (eV)	NTO[c] Hole	Electron	Population	E_{eb}[d] (eV)	EHS[e]	L (Å)	t (Å)
AJ1-DPA	2.354	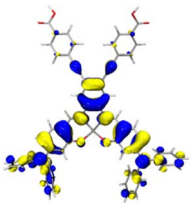	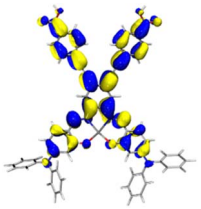	99.2%	2.401	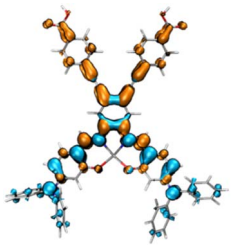	4.622	0.347
AJ1-TPA	2.214	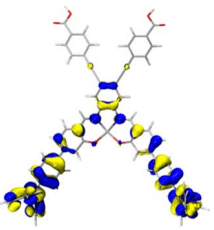	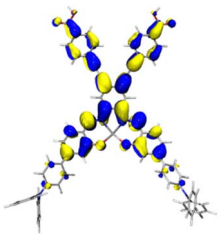	98.6%	1.662	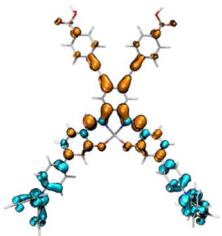	8.007	3.632
AJ2-AN	1.987	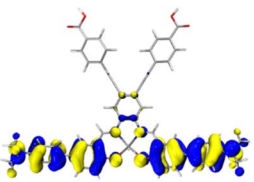	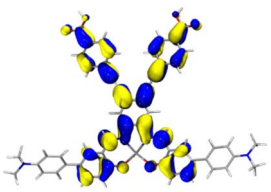	99.5%	2.125	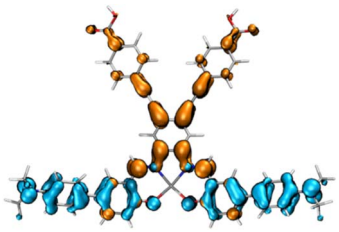	4.879	1.910
AJ2-DPA	1.882	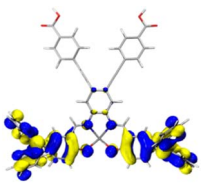	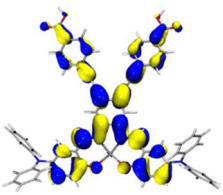	98.7%	2.342	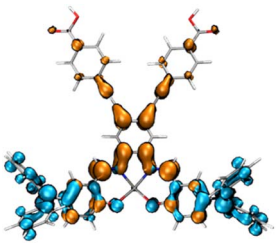	3.933	0.912
AJ2-TPA	1.997	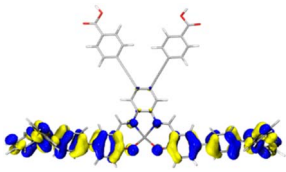	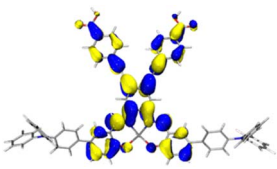	99.2%	1.918	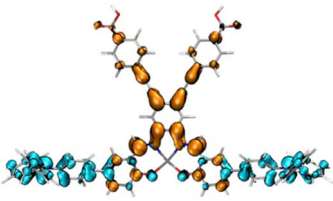	4.708	1.837

[a] The results were computed at the TD-B3LYP/6-311G(d,p) level of theory and the orbitals were plotted with isovalue = 0.05. [b] E_{cal} denotes to the lowest-energy vertical excitations. [c] The NTOs shown account for >98.6% of the respective total excitation process. [d] E_{eb} denotes to exciton binding energy. [e] Those orbitals colored in blue represent depletion of electron density, while that in orange represent increment of electron density. L represents the charge transfer distance. The t index represents the degree of electron–hole separation.

to AN- and TPA-derivatives, leading to less favorable intramolecular charge transfer of DPA-containing dyes. For instance, the **CL**-series dyes possess computed L of the trend **CL-DPA** (4.887) < **CL-AN** (6.445) < **CL-TPA** (7.868). The same observation was obtained for the parameter t corresponding to electron–hole separation. This fact clearly explains the aforementioned trend observed for predicted UV-vis absorption (*vide supra*). Furthermore, the more red-shifted **AJ2**-series dyes appear to have calculated L and t indexes relatively shorter than that for **AJ1**-, **YD**-, **CL**-series dyes. The fact is possibly due to orthogonal

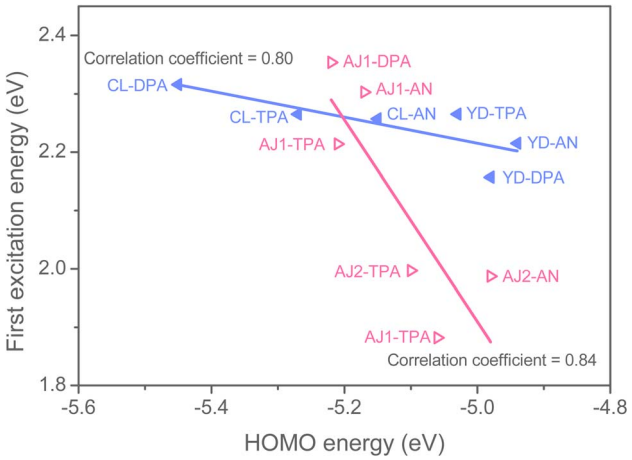

Fig. 7 Correlation of HOMO energies with the first excitation energies for ZSC molecules.

orientation of two D and one A groups in π-shaped **AJ2**-dyes. By using EHS approach, center of mass for the hole density will be in a close proximity with that for electron density in **AJ2**-series dyes, leading to underestimation of separation indexes.

Finally, the population of mono-cationic charge within a dye were monitored, as shown in Fig. S7.† In the case of DPA-derivatives, the four series of dyes show substantial accumulation of positive charge at ZnS moieties. For TPA- and AN-derivatives, on the other hand, the positive charge is evenly populated at both arylamine and ZnS moieties. The difference in cationic charge population is considered to bring certain impact on dye regeneration.[47]

Conclusion

In summary, this work focuses on density functional and time-dependent density functional approaches for examining four series of zinc-salophen complexes (ZSC) as novel dye system toward dye-sensitized solar cell (DSSC) applications. The regio-specificity was found clearly for these ZSC dyes in terms of HOMO energies, vertical excitations, and charge transfer properties. The **AJ2**-series dyes with disubstituted anilines (AN), diphenylamines (DPA), and triphenylamines (TPA) all exhibit much broader UV-Vis absorption together with red-shifted λ_{max}, compared to **AJ1**-, **YD**-, and **CL**-series dyes. The **AJ1**-series dyes have the absorption with the largest extinction coefficients when compared to the rest series of dyes, as concluded from the calculations at gas-phased B3LYP/6-311G** level. With the *para*-ethynylbenzoic acids (EBAs) functionalized at phenyl-enediimine 7,8-positions, there exists significant linear relationship between HOMO energies and lowest-energy excitation energies (E_{cal}), as shown in the case of **AJ1**- and **AJ2**-series dyes. In a different manner, when EBAs are functionalized at phen-oxide 3,12,2,13-positions, the corresponding E_{cal} does not notably affected by varied HOMO energies which in turn originated from substitution of different donor groups. All the ZSC dyes in this study have HOMO energies (from −4.94 eV to −5.76 eV) lower than the reference dye **YD2-o-C8** (−4.83 eV). This enables the employment of cobalt(II/II)- and copper(I/II)-based electrolytes with higher redox potentials such that DSSC devices with larger theoretical open-circuit voltage (V_{OC}) can be achieved. Furthermore, as evidenced in the frontier MOs, functionalization of zinc-salophen (ZnS) moiety at 7,8-positions will have dominate and minor influences on HOMO and LUMO energy levels, respectively. Whereas functionalization at ZnS 2,13,3,12-positions will have influences primarily at LUMO level. Consequently, substitution of EBAs and varied donor groups at difference positions, as exampled by **YD**-, **CL**-, **AJ1**-, and **AJ2**-series dyes, will result in different outcome concerning HOMO energy levels and calculated E_{cal} as illustrated in the table shown in Fig. 8. Finally, NTO approach reveals that the **CL**-, **AJ1**-, and **AJ2**-series dyes show lowest-energy excitations with sufficient charge transfer properties leading to efficient electron injection, while **YD**-series dyes do not. In the case of **CL**- and **AJ1**-series dyes, electron–hole separation (EHS) approach displays that the DPA-derivatives have shorter charge transfer distances (L) than AN- and TPA-derivatives, showing poorer intramolecular charge transfer properties. The calculated exciton binding energy (E_{eb}) confirms the strength of CT character in a trend of TPA-derivatives > AN-derivatives > DPA-derivatives.

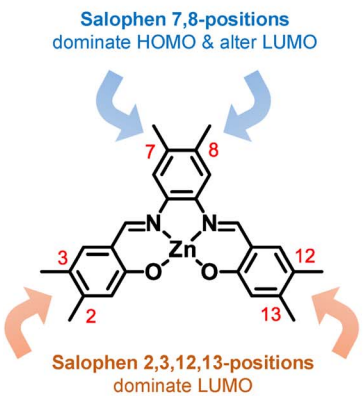

	EBA positions	Am positions	Bandgap
AJ1/AJ2	Top fixed HOMO; altered LUMO	Bottom varied LUMO	varied
CL	Bottom fixed LUMO	Top varied HOMO; altered LUMO	fixed
YD	Bottom fixed LUMO	Bottom (methoxy on top) fixed HOMO; altered LUMO	fixed

Fig. 8 Influences of Am- and EBA-substitution on molecular properties of ZSC dyes.

Computational details

The ground-state geometries of the dyes were optimized using B3LYP with the 6-311G(d,p) basis set for all the molecules. When noted in the main text, modeling of the solvent effect in THF was taken into account by means of the conductor-like polarizable continuum model (C-PCM) and tetrahydrofuran ($\varepsilon = 7.4257$) as the medium.[79] Frequency calculations were carried out at the same level of theory as geometry optimization to confirm successful optimization of the geometries to stable points. Time-dependent density functional theory (TDDFT) calculations were performed on all molecules using 6-311G** basis sets, while hybrid functional, B3LYP, as well as range-separated functional, LC-PBE0, wB97XD, and LC-BLYP were employed both with and without the inclusion of C-PCM. We also evaluated the ω values of LRC functionals where 0% Hartree-Fock exists in the short-range to probe the suitable short-range criteria for non-Coulomb part of exchange. The range–separation parameter ω was set to 0.30, 0.30 and 0.47 a.u. for LC-BLYP, CAM-B3LYP and wB97XD functional following the scheme described in the literature.[66] All calculations were performed with the Gaussian 16 program package.[80] The resultant vertical excitation profile is followed by simulation of absorption spectra using SWizard software with a full width at half maximum of 3000 cm^{-1}.[81] Natural transition orbital (NTO), intramolecular charge-transfer characteristics, charge density difference plots, and exciton binding energy were analyzed with Multiwfn program[82] to compare the abilities of charge transfer.

Conflicts of interest

The authors declare no competing financial interest.

Acknowledgements

The authors thank the financial support for this work from the National Science and Technology Council (NSTC) in Taiwan with Grant No. MOST 108-2113-M-126 -002 -MY3. We thank to National Center for High-performance Computing (NCHC) of National Applied Research Laboratories (NARLabs) in Taiwan for providing computational and storage resources.

References

1 N. S. Lewis and D. G. Nocera, *Proc. Natl. Acad. Sci. U. S. A.*, 2006, **103**, 15729–15735.
2 J. Y. Kim, J.-W. Lee, H. S. Jung, H. Shin and N.-G. Park, *Chem. Rev.*, 2020, **120**, 7867–7918.
3 Z. Guo, A. K. Jena, G. M. Kim and T. Miyasaka, *Energy Environ. Sci.*, 2022, **15**, 3171–3222.
4 A. B. Muñoz-García, I. Benesperi, G. Boschloo, J. J. Concepcion, J. H. Delcamp, E. A. Gibson, G. J. Meyer, M. Pavone, H. Pettersson, A. Hagfeldt and M. Freitag, *Chem. Soc. Rev.*, 2021, **50**, 12450–12550.
5 M. Kokkonen, P. Talebi, J. Zhou, S. Asgari, S. A. Soomro, F. Elsehrawy, J. Halme, S. Ahmad, A. Hagfeldt and S. G. Hashmi, *J. Mater. Chem. A*, 2021, **9**, 10527–10545.
6 K. A. Mazzio and C. K. Luscombe, *Chem. Soc. Rev.*, 2014, **44**, 78–90.
7 P. Cheng, G. Li, X. Zhan and Y. Yang, *Nat. Photonics*, 2018, **12**, 131–142.
8 I. Mora-Seró, *Adv. Energy Mater.*, 2020, **10**, 2001774.
9 Z. Pan, H. Rao, I. Mora-Seró, J. Bisquert and X. Zhong, *Chem. Soc. Rev.*, 2018, **47**, 7659–7702.
10 H. Michaels, I. Benesperi and M. Freitag, *Chem. Sci.*, 2021, **12**, 5002–5015.
11 S. Yun, Y. Qin, A. R. Uhl, N. Vlachopoulos, M. Yin, D. Li, X. Han and A. Hagfeldt, *Energy Environ. Sci.*, 2018, **11**, 476–526.
12 M. Grätzel, *Inorg. Chem.*, 2005, **44**, 6841–6851.
13 M. Grätzel, *J. Photochem. Photobiol., A*, 2004, **164**, 3–14.
14 A. Yella, C.-L. Mai, S. M. Zakeeruddin, S.-N. Chang, C.-H. Hsieh, C.-Y. Yeh and M. Grätzel, *Angew. Chem., Int. Ed.*, 2014, **53**, 2973–2977.
15 S. Mathew, A. Yella, P. Gao, R. Humphry-Baker, B. F. E. Curchod, N. Ashari-Astani, I. Tavernelli, U. Rothlisberger, M. K. Nazeeruddin and M. Grätzel, *Nat. Chem.*, 2014, **6**, 242–247.
16 S. H. Kang, M. J. Jeong, Y. K. Eom, I. T. Choi, S. M. Kwon, Y. Yoo, J. Kim, J. Kwon, J. H. Park and H. K. Kim, *Adv. Energy Mater.*, 2017, **7**, 1602117.
17 K. Zeng, Y. Chen, W.-H. Zhu, H. Tian and Y. Xie, *J. Am. Chem. Soc.*, 2020, **142**, 5154–5161.
18 C.-C. Chen, J.-S. Chen, V. S. Nguyen, T.-C. Wei and C.-Y. Yeh, *Angew. Chem., Int. Ed.*, 2021, **60**, 4886–4893.
19 K. Zeng, Z. Tong, L. Ma, W.-H. Zhu, W. Wu and Y. Xie, *Energy Environ. Sci.*, 2020, **13**, 1617–1657.
20 J. Lu, S. Liu and M. Wang, *Front. Chem.*, 2018, **6**, 541.
21 M. Urbani, M. Grätzel, M. K. Nazeeruddin and T. Torres, *Chem. Rev.*, 2014, **114**, 12330–12396.
22 Y. Wu and W. Zhu, *Chem. Soc. Rev.*, 2013, **42**, 2039–2058.
23 S. A. Ok, B. Jo, S. Somasundaram, H. J. Woo, D. W. Lee, Z. Li, B.-G. Kim, J. H. Kim, Y. J. Song, T. K. Ahn, S. Park and H. J. Park, *Nat. Commun.*, 2018, **9**, 4537.
24 Y. Wang, Q. Liao, J. Chen, W. Huang, X. Zhuang, Y. Tang, B. Li, X. Yao, X. Feng, X. Zhang, M. Su, Z. He, T. J. Marks, A. Facchetti and X. Guo, *J. Am. Chem. Soc.*, 2020, **142**, 16632–16643.
25 M. F. M. Kavungathodi, I. Cho, P. Wagner and A. J. Mozer, *J. Phys. Chem. C*, 2020, **124**, 23013–23026.
26 G. Boschloo and A. Hagfeldt, *Acc. Chem. Res.*, 2009, **42**, 1819–1826.
27 M. Wang, C. Grätzel, S. M. Zakeeruddin and M. Grätzel, *Energy Environ. Sci.*, 2012, **5**, 9394–9405.
28 J. M. Cole, G. Pepe, O. K. Al Bahri and C. B. Cooper, *Chem. Rev.*, 2019, **119**, 7279–7327.
29 T. M. Koh, K. Nonomura, N. Mathews, A. Hagfeldt, M. Grätzel, S. G. Mhaisalkar and A. C. Grimsdale, *J. Phys. Chem. C*, 2013, **117**, 15515–15522.
30 C. Zhang, Y. Huang, Z. Huo, S. Chen and S. Dai, *J. Phys. Chem. C*, 2009, **113**, 21779–21783.
31 C. Lin, F.-Y. Tsai, M.-H. Lee, C.-H. Lee, T.-C. Tien, L.-P. Wang and S.-Y. Tsai, *J. Mater. Chem.*, 2009, **19**, 2999–3003.

32 H. Yu, B. Xue, P. Liu, J. Qiu, W. Wen, S. Zhang and H. Zhao, *ACS Appl. Mater. Interfaces*, 2012, **4**, 1289–1294.
33 N. Koumura, Z.-S. Wang, S. Mori, M. Miyashita, E. Suzuki and K. Hara, *J. Am. Chem. Soc.*, 2006, **128**, 14256–14257.
34 A. Abbotto, N. Manfredi, C. Marinzi, F. De Angelis, E. Mosconi, J.-H. Yum, Z. Xianxi, M. K. Nazeeruddin and M. Grätzel, *Energy Environ. Sci.*, 2009, **2**, 1094.
35 R. Ambre, K.-B. Chen, C.-F. Yao, L. Luo, E. W.-G. Diau and C.-H. Hung, *J. Phys. Chem. C*, 2012, **116**, 11907–11916.
36 W.-I. Hung, Y.-Y. Liao, T.-H. Lee, Y.-C. Ting, J.-S. Ni, W.-S. Kao, J. T. Lin, T.-C. Wei and Y.-S. Yen, *Chem. Commun.*, 2015, **51**, 2152–2155.
37 Y.-S. Yen, J.-S. Ni, T.-Y. Lin, W.-I. Hung, J. T. Lin and M.-C. P. Yeh, *Eur. J. Org. Chem.*, 2015, **33**, 7367–7377.
38 F. De Angelis, S. Fantacci, A. Selloni, M. Grätzel and M. K. Nazeeruddin, *Nano Lett.*, 2007, **7**, 3189–3195.
39 R. B. Ambre, G.-F. Chang and C.-H. Hung, *Chem. Commun.*, 2014, **50**, 725–727.
40 Y. Jia, F. Gou, R. Fang, H. Jing and Z. Zhu, *Chin. J. Chem.*, 2014, **32**, 513–520.
41 L. Zheng, T. H. Hurst, Z. Li, X. Zheng, C. C. Nnyamah and L. V. Wrensford, *Nano Express*, 2020, **1**, 010040.
42 J. Zhang, A. Zhong, G. Huang, M. Yang, D. Li, M. Teng and D. Han, *Sol. Energy*, 2020, **209**, 316–324.
43 S. Yang, H. Kou, H. Wang, K. Cheng and J. Wang, *New J. Chem.*, 2010, **34**(2), 313–317.
44 M. Pastore and F. De Angelis, *J. Phys. Chem. Lett.*, 2013, **4**, 956–974.
45 Y. Mao, M. Head-Gordon and Y. Shao, *Chem. Sci.*, 2018, **9**, 8598–8607.
46 H. Bronstein, C. B. Nielsen, B. C. Schroeder and I. McCulloch, *Nat. Rev. Chem.*, 2020, **4**, 66–77.
47 H.-H. Chou, K. S. K. Reddy, H.-P. Wu, B.-C. Guo, H.-W. Lee, E. W.-G. Diau, C.-P. Hsu and C.-Y. Yeh, *ACS Appl. Mater. Interfaces*, 2016, **8**, 3418–3427.
48 Z. Zheng, Y. Shao, C. Ding, M. Li and W. Lu, *J. Mol. Struct.*, 2022, **1269**, 133728.
49 Y. Ren, Y. Li, S. Chen, J. Liu, J. Zhang and P. Wang, *Energy Environ. Sci.*, 2016, **9**, 1390–1399.
50 A. Yella, H.-W. Lee, H. N. Tsao, C. Yi, A. K. Chandiran, M. K. Nazeeruddin, E. W.-G. Diau, C.-Y. Yeh, S. M. Zakeeruddin and M. Gratzel, *Science*, 2011, **334**, 629–634.
51 S. R. Bora and D. J. Kalita, *RSC Adv.*, 2021, **11**, 39246–39261.
52 L. Leoni, A. Carletta, L. Fusaro, J. Dubois, N. A. Tumanov, C. Aprile, J. Wouters and A. Dalla Cort, *Molecules*, 2019, **24**, 2314.
53 L. G. T. A. Duarte, J. C. Germino, R. A. Mendes, J. F. Berbigier, K. S. Moreira, M. M. Faleiros, J. N. de Freitas, T. A. L. Burgo, F. S. Rodembusch and T. D. Z. Atvars, *J. Phys. Chem. C*, 2020, **124**, 21036–21046.
54 P. A. Prasanth, P. Nantheeswaran, V. Anbazhagan, R. Senthilnathan, A. Jothi, N. S. P. Bhuvanesh, L. K. Sannegowda and M. Mariappan, *New J. Chem.*, 2020, **44**, 9888–9895.
55 E. Mosconi, J.-H. Yum, F. Kessler, C. J. Gómez García, C. Zuccaccia, A. Cinti, M. K. Nazeeruddin, M. Grätzel and F. De Angelis, *J. Am. Chem. Soc.*, 2012, **134**, 19438–19453.
56 J. An, X. Yang, B. Cai, L. Zhang, K. Yang, Z. Yu, X. Wang, A. Hagfeldt and L. Sun, *ACS Appl. Mater. Interfaces*, 2020, **12**, 46397–46405.
57 B. Selvaraj, G. Shanmugam, S. Kamaraj, A. Gunasekeran and A. Sambandam, *Inorg. Chem.*, 2021, **60**, 1937–1947.
58 K. Kannankutty, C.-C. Chen, V. S. Nguyen, Y.-C. Lin, H.-H. Chou, C.-Y. Yeh and T.-C. Wei, *ACS Appl. Mater. Interfaces*, 2020, **12**, 5812–5819.
59 S. O. Fürer, R. A. Milhuisen, M. K. Kashif, S. R. Raga, S. S. Acharya, C. Forsyth, M. Liu, L. Frazer, N. W. Duffy, C. A. Ohlin, A. M. Funston, Y. Tachibana and U. Bach, *Adv. Energy Mater.*, 2020, **10**, 2002067.
60 M. Freitag, J. Teuscher, Y. Saygili, X. Zhang, F. Giordano, P. Liska, J. Hua, S. M. Zakeeruddin, J.-E. Moser, M. Grätzel and A. Hagfeldt, *Nat. Photonics*, 2017, **11**, 372–378.
61 F. Gao, C.-L. Yang, M.-S. Wang, X.-G. Ma and W.-W. Liu, *Spectrochim. Acta, Part A*, 2018, **195**, 176–183.
62 W. R. Duncan and O. V. Prezhdo, *Annu. Rev. Phys. Chem.*, 2007, **58**, 143–184.
63 F. Dumur, E. Contal, G. Wantz and D. Gigmes, *Eur. J. Inorg. Chem.*, 2014, **25**, 4186–4198.
64 C.-R. Zhang, J. S. Sears, B. Yang, S. G. Aziz, V. Coropceanu and J.-L. Brédas, *J. Chem. Theory Comput.*, 2014, **10**, 2379–2388.
65 Z.-Q. You, Y.-C. Hung and C.-P. Hsu, *J. Phys. Chem. B*, 2015, **119**, 7480–7490.
66 H.-H. Chou, C.-H. Yang, J. T. Lin and C.-P. Hsu, *J. Phys. Chem. C*, 2017, **121**, 983–992.
67 M. Rezvani, M. Darvish Ganji, S. Jameh-Bozorghi and A. Niazi, *Spectrochim. Acta, Part A*, 2018, **194**, 57–66.
68 M. Tale Moghim, S. Jamehbozorgi, M. Rezvani and M. Ramezani, *Spectrochim. Acta, Part A*, 2022, **280**, 121488.
69 J. Watson, T. J. Santaloci, H. Cheema, R. C. Fortenberry and J. H. Delcamp, *J. Phys. Chem. C*, 2020, **124**, 25211–25220.
70 T.-H. Lee, C.-Y. Hsu, Y.-Y. Liao, H.-H. Chou, H. Hughes and J. T. Lin, *Chem.–Asian J.*, 2014, **9**, 1933–1942.
71 S. Karthikeyan and J. Y. Lee, *J. Phys. Chem. A*, 2013, **117**, 10973–10979.
72 F. Gao, C.-L. Yang, M.-S. Wang, X.-G. Ma and W.-W. Liu, *Spectrochim. Acta, Part A*, 2019, **216**, 69–75.
73 D. Vijay, E. Varathan and V. Subramanian, *J. Mater. Chem. A*, 2013, **1**, 4358.
74 P. J. Leenaers, A. J. L. A. Maufort, M. M. Wienk and R. A. J. Janssen, *J. Phys. Chem. C*, 2020, **124**, 27403–27412.
75 S. Kraner, G. Prampolini and G. Cuniberti, *J. Phys. Chem. C*, 2017, **121**, 17088–17095.
76 S. Kraner, R. Scholz, F. Plasser, C. Koerner and K. Leo, *J. Chem. Phys.*, 2015, **143**, 244905.
77 F. Mendizabal, R. Mera-Adasme, W.-H. Xu and D. Sundholm, *RSC Adv.*, 2017, **7**, 42677–42684.
78 Z. Liu, T. Lu and Q. Chen, *Carbon*, 2020, **165**, 461–467.
79 J. Tomasi, B. Mennucci and R. Cammi, *Chem. Rev.*, 2005, **105**, 2999–3094.

80 M. J. Frisch, G. W. Trucks, H. B. Schlegel, G. E. Scuseria, M. A. Robb, J. R. Cheeseman, G. Scalmani, V. Barone, G. A. Petersson, H. Nakatsuji, X. Li, M. Caricato, A. V. Marenich, J. Bloino, B. G. Janesko, R. Gomperts, B. Mennucci, H. P. Hratchian, J. V. Ortiz, A. F. Izmaylov, J. L. Sonnenberg, D. Williams-Young, F. Ding, F. Lipparini, F. Egidi, J. Goings, B. Peng, A. Petrone, T. Henderson, D. Ranasinghe, V. G. Zakrzewski, J. Gao, N. Rega, G. Zheng, W. Liang, M. Hada, M. Ehara, K. Toyota, R. Fukuda, J. Hasegawa, M. Ishida, T. Nakajima, Y. Honda, O. Kitao, H. Nakai, T. Vreven, K. Throssell, J. A. Montgomery Jr, J. E. Peralta, F. Ogliaro, M. J. Bearpark, J. J. Heyd, E. N. Brothers, K. N. Kudin, V. N. Staroverov, T. A. Keith, R. Kobayashi, J. Normand, K. Raghavachari, A. P. Rendell, J. C. Burant, S. S. Iyengar, J. Tomasi, M. Cossi, J. M. Millam, M. Klene, C. Adamo, R. Cammi, J. W. Ochterski, R. L. Martin, K. Morokuma, O. Farkas, J. B. Foresman and D. J. Fox, *Gaussian 16 Rev. B.01*, 2016.
81 S. I. Gorelsky and A. B. P. Lever, *J. Organomet. Chem.*, 2001, **635**, 187–196.
82 T. Lu and F. Chen, *J. Comput. Chem.*, 2012, **33**, 580–592.